

A Semi-Implicit Runge–Kutta Time-Difference Scheme for the Two-Dimensional Shallow-Water Equations

SAJAL K. KAR

I. M. Systems Group, Inc., Kensington, Maryland

(Manuscript received 20 April 2005, in final form 13 January 2006)

ABSTRACT

A semi-implicit, two time-level, three-step iterative time-difference scheme is proposed for the two-dimensional nonlinear shallow-water equations in a conservative flux form. After a semi-implicit linearization of the governing equations, the linear gravity wave terms are time discretized implicitly using a second-order trapezoidal scheme applied over each iterative step, whereas the nonlinear terms including horizontal advection and other terms left over from the semi-implicit linearization are time discretized explicitly using a third-order Runge–Kutta scheme. The effectiveness of the scheme in terms of numerical accuracy, stability, and efficiency is established through a forced initial-boundary value problem studied using a two-dimensional shallow-water model.

1. Introduction

Two-time-level Runge–Kutta schemes of the third and fourth order (hereafter RK3 and RK4) have been widely used in computational fluid dynamics, but not in atmospheric numerical weather prediction (NWP). The traditional scheme of choice in atmospheric NWP has been the three-time-level leapfrog scheme, which is formally second-order accurate in time with a rather restricted Courant–Friedrichs–Lewy (CFL) limit on the time step for linear computational stability. Unfortunately, the leapfrog scheme also includes a computational mode in time that is usually controlled by a time filter (Asselin 1972), which makes the time-filtered leapfrog scheme only first-order accurate. In spite of these limitations, the leapfrog scheme continues to be used in various NWP models, because it is easy to code and needs only one evaluation of the right side of prognostic equations per time step.

Compared to the leapfrog scheme, the RK3 and RK4 schemes have two advantages: (a) being based on two time levels, the RK schemes do not have a computational mode in time, and (b) the RK schemes have more relaxed CFL restrictions that allow relatively large time steps (Durran 1999, 68–69). Mathematical development

and numerical properties of the Runge–Kutta family of schemes, in general, can be found in a number of textbooks including Butcher (1987) and Gear (1971). The main disadvantage of the RK3 and RK4 schemes, compared to the time-filtered leapfrog scheme, is that they, respectively, require three and four evaluations of the right side of the prognostic equations per time step. Primarily for this reason, until recently the RK3 and RK4 schemes have not been widely used in atmospheric NWP models.

Recently, Wicker and Skamarock (2002) have suggested that the RK3 scheme can be an “excellent” choice in terms of numerical accuracy, stability, and efficiency for atmospheric NWP models. In fact, they have developed a time-split form of the explicit RK3 scheme that employs relatively small and large time steps for the high-frequency modes (primarily acoustic and gravity–inertia waves) and low-frequency meteorological modes (primarily advection), respectively. The time-split RK3 scheme is currently being used in the Advanced Research Weather Research and Forecast (WRF) model (Skamarock et al. 2001).

An established alternative to the split-explicit time-differencing approach adopted by Skamarock et al. (2001) is the semi-implicit time-differencing scheme (Robert 1969; Kwizak and Robert 1971) that employs a trapezoidal implicit scheme for the high-frequency modes mentioned above. The semi-implicit time-difference scheme, in contrast to a fully explicit scheme,

Corresponding author address: Dr. Sajal K. Kar, W/NP2, Rm. 207, WWBG, 5200 Auth Rd., Camp Springs, MD 20746-4304.
E-mail: sajal.kar@noaa.gov

eliminates the CFL restriction on time step imposed by the high-frequency modes. Thus, in terms of numerical efficiency, the semi-implicit scheme provides an alternative to the split-explicit scheme mentioned earlier.

In this paper, a semi-implicit Runge–Kutta scheme is developed for the two-dimensional nonlinear shallow-water equations in flux convergence form. As noted by a reviewer, there is a growing body of implicit and semi-implicit Runge–Kutta schemes available in the literature. For example, Ascher et al. (1997) has proposed a family of semi-implicit Runge–Kutta schemes applied to the advection–diffusion equation; Butcher (1964) has developed fully implicit Runge–Kutta schemes that require a simultaneous solution of equations at each time step. We have not explored such alternative approaches prior to developing the semi-implicit Runge–Kutta scheme proposed here.

In section 2, we present the mathematical derivation of the scheme, followed by some numerical results that compare the semi-implicit RK scheme to the explicit RK3 scheme and to the time-filtered semi-implicit leap-frog scheme. A summary is presented in section 3. Finally, a linear stability analysis of the proposed scheme is presented in the appendix.

2. The semi-implicit Runge–Kutta time-difference scheme

a. Formulation of the scheme in a space-continuous form

Let us consider a generic tendency equation:

$$\frac{\partial \Psi}{\partial t} = F(\Psi), \tag{2.1}$$

where Ψ is an arbitrary prognostic variable that is a function of space and time. The explicit RK3 (hereafter expRK3) time-difference scheme for (2.1) is expressed as follows.

stage 1,

$$\Psi^* = \Psi^n + \frac{\Delta t}{3} F^n; \tag{2.2}$$

stage 2,

$$\Psi^{**} = \Psi^n + \frac{\Delta t}{2} F^*; \text{ and} \tag{2.3}$$

stage 3,

$$\Psi^{n+1} = \Psi^n + \Delta t F^{**}; \tag{2.4}$$

where $F^* \equiv F(\Psi^*)$ and $F^{**} \equiv F(\Psi^{**})$. Here the superscripts n and $n + 1$ denote the time-level indices, while Δt is the time step. The superscripted asterisk (*)

and double asterisk (**) denote the “provisional” time-level indices. This particular form of the explicit RK3 scheme has also been adopted by Wicker and Skamarock (2002). However, there are many other possible forms of the explicit RK3 schemes (see Butcher 1987) that have not been explored in this paper.

Notice that the RK3 scheme given above is an explicit, three-step, iterative, two-level time-difference scheme. In this scheme, (2.2) represents a predictor step that is a forward scheme with a time step of $\Delta t/3$ over the time interval $[n\Delta t, (n + 1/3)\Delta t]$, (2.3) represents another predictor step that is a centered scheme with a time step of $\Delta t/2$ over the time interval $[n\Delta t, (n + 1/2)\Delta t]$, and (2.4) represents a corrector step that is also a centered scheme with a time step of Δt over the time interval $[n\Delta t, (n + 1)\Delta t]$. Thus, the three iterative steps of the explicit RK3 scheme can be rewritten in a compact form,

$$\frac{\Psi^{n+\delta_k} - \Psi^n}{\delta_k \Delta t} = F(\Psi^{n+\delta_{k-1}}) \equiv F^{n+\delta_{k-1}}, \tag{2.5}$$

where the subscript $k = [1, 2, 3]$ denotes the three steps of the RK3 scheme and $\{\delta_k\}$ is a sequence of real constants:

$$\delta_0 = 0, \quad \delta_1 = 1/3, \quad \delta_2 = 1/2, \quad \delta_3 = 1. \tag{2.6}$$

For a semi-implicit extension of the explicit RK3 scheme, we first rewrite the generic tendency Eq. (2.1) as

$$\frac{\partial \Psi}{\partial t} = F(\Psi) = L(\Psi) + N(\Psi), \tag{2.7}$$

where L and N denote the “linear” and “nonlinear” parts of F . This semi-implicit linearization of F is done with respect to a time-independent reference state. In general, the linear part L represents the high-frequency wave solutions and the nonlinear part N represents the low-frequency solutions representing advection and other processes. For the proposed semi-implicit RK3 (hereafter siRK3) scheme, we employ a trapezoidal scheme for the linear part L and the expRK3 scheme for the nonlinear part N . Thus, in view of (2.5), the three steps [$k = 1, 2, 3$] of the siRK3 scheme for (2.1) can be written in a compact form:

$$\frac{\Psi^{n+\delta_k} - \Psi^n}{\delta_k \Delta t} = \frac{1}{2} [(1 + \varepsilon_g)L^{n+\delta_k} + (1 - \varepsilon_g)L^n] + N^{n+\delta_{k-1}}, \tag{2.8}$$

where ε_g is the uncentering parameter restricted by $0 \leq \varepsilon_g \leq 1$. Here, $\varepsilon_g = 0$ represents the trapezoidal scheme that is second-order accurate, and $\varepsilon_g = 1$ represents the

backward scheme that is first-order accurate. Introducing the real constants γ_k^+ and γ_k^- , defined by

$$\gamma_k^+ \equiv \frac{1}{2}(1 + \varepsilon_g)\delta_k\Delta t; \quad \gamma_k^- \equiv \frac{1}{2}(1 - \varepsilon_g)\delta_k\Delta t$$

$$\forall k = 1, 2, 3, \quad (2.9)$$

we can rewrite (2.8) as

$$\Psi^{n+\delta_k} - \Psi^n = \gamma_k^+ L^{n+\delta_k} + \gamma_k^- L^n + (\delta_k\Delta t)N^{n+\delta_{k-1}},$$

or

$$\Psi^{n+\delta_k} - \gamma_k^+ L^{n+\delta_k} = \Psi^n + \gamma_k^- L^n + (\delta_k\Delta t)N^{n+\delta_{k-1}} \equiv R_k$$

$$\forall k = 1, 2, 3. \quad (2.10)$$

The set of three equations given by (2.10) constitutes the siRK3 scheme. Quite like the semi-implicit leapfrog scheme (Kwizak and Robert 1971), the siRK3 scheme is conditionally stable. The CFL restriction on Δt is basically dictated by the expRK3 scheme used for the slow-moving (e.g., advective) processes. A traditional von Neumann stability analysis of the siRK3 scheme is presented in the appendix. Next, we apply the siRK3 scheme to the two-dimensional shallow-water equations.

The 2D nonlinear shallow-water equations in Cartesian coordinates (x, y) can be expressed in a *flux convergence* form:

$$\frac{\partial U}{\partial t} = fV - \left[\frac{\partial}{\partial x}(Uu) + \frac{\partial}{\partial y}(Uv) \right] - g \frac{\partial}{\partial x} \left(\frac{1}{2} \xi^2 \right) + \xi F_x, \quad (2.11)$$

$$\frac{\partial V}{\partial t} = -fU - \left[\frac{\partial}{\partial x}(Vu) + \frac{\partial}{\partial y}(Vv) \right] - g \frac{\partial}{\partial y} \left(\frac{1}{2} \xi^2 \right) + \xi F_y, \quad \text{and} \quad (2.12)$$

$$\frac{\partial \xi}{\partial t} = - \left(\frac{\partial U}{\partial x} + \frac{\partial V}{\partial y} \right) + S, \quad (2.13)$$

where

$$U \equiv \xi u, \quad V \equiv \xi v, \quad f(y) = f_0 + \beta y. \quad (2.14)$$

Here, u and v denote the velocity components in x and y directions, respectively, and ξ denotes the depth of the free surface; F_x and F_y denote the friction in x and y directions, respectively, and S denotes the source or sink of mass. For the semi-implicit linearization of the shallow-water equations, we express the depth of the free surface as

$$\xi = H + h, \quad (2.15)$$

where H and h denote the mean depth of the shallow layer and the perturbation depth of the free surface from H . Then the system (2.11)–(2.13) is expressed as

$$\frac{\partial U}{\partial t} + gH \frac{\partial h}{\partial x} = N_u, \quad (2.16)$$

$$\frac{\partial V}{\partial t} + gH \frac{\partial h}{\partial y} = N_v, \quad \text{and} \quad (2.17)$$

$$\frac{\partial h}{\partial t} + \left(\frac{\partial U}{\partial x} + \frac{\partial V}{\partial y} \right) = N_h, \quad (2.18)$$

where

$$N_u \equiv - \left[\frac{\partial(Uu)}{\partial x} + \frac{\partial(Uv)}{\partial y} \right] + fV - \frac{g}{2} \frac{\partial h^2}{\partial x} + \xi F_x, \quad (2.19)$$

$$N_v \equiv - \left[\frac{\partial(Vu)}{\partial x} + \frac{\partial(Vv)}{\partial y} \right] - fU - \frac{g}{2} \frac{\partial h^2}{\partial y} + \xi F_y, \quad \text{and} \quad (2.20)$$

$$N_h \equiv S. \quad (2.21)$$

As an intended consequence of the semi-implicit linearization, the homogeneous system (2.16)–(2.18) governs the free-surface pure gravity waves with the uniform phase speed $c_g \equiv (gH)^{1/2}$.

In view of the similarity between (2.7) and each of (2.16)–(2.18), we obtain an analog of (2.10) for each of the linearized shallow-water equations as

$$U^{n+\delta_k} + \gamma_k^+ gH \frac{\partial h^{n+\delta_k}}{\partial x} = (R_u)_k, \quad (2.22)$$

$$V^{n+\delta_k} + \gamma_k^+ gH \frac{\partial h^{n+\delta_k}}{\partial y} = (R_v)_k, \quad \text{and} \quad (2.23)$$

$$h^{n+\delta_k} + \gamma_k^+ \left(\frac{\partial U^{n+\delta_k}}{\partial x} + \frac{\partial V^{n+\delta_k}}{\partial y} \right) = (R_h)_k, \quad (2.24)$$

where

$$(R_u)_k \equiv U^n - \gamma_k^- gH \frac{\partial h^n}{\partial x} + (\delta_k\Delta t)N_u^{n+\delta_{k-1}}, \quad (2.25)$$

$$(R_v)_k \equiv V^n - \gamma_k^- gH \frac{\partial h^n}{\partial y} + (\delta_k\Delta t)N_v^{n+\delta_{k-1}}, \quad \text{and} \quad (2.26)$$

$$(R_h)_k \equiv h^n - \gamma_k^- \left(\frac{\partial U^n}{\partial x} + \frac{\partial V^n}{\partial y} \right) + (\delta_k\Delta t)N_h^{n+\delta_{k-1}}. \quad (2.27)$$

Equations (2.22)–(2.24) applied in three successive steps with $k = 1, 2, 3$, constitute the siRK3 time-

difference scheme for the shallow-water equations in a space-continuous form. For a computational implementation of the scheme, we eliminate the unknown variables $U^{n+\delta_k}$ and $V^{n+\delta_k}$ between (2.22), (2.23), and (2.24), and obtain a Helmholtz-type elliptic equation for the unknown variable, $h^{n+\delta_k}$:

$$\left(\frac{\partial^2}{\partial x^2} + \frac{\partial^2}{\partial y^2}\right)h^{n+\delta_k} - \frac{h^{n+\delta_k}}{gH(\gamma_k^+)^2} = \frac{1}{gH(\gamma_k^+)^2} \left\{ \gamma_k^+ \left[\frac{\partial(R_u)_k}{\partial x} + \frac{\partial(R_v)_k}{\partial y} \right] - (R_h)_k \right\} \equiv \mathfrak{R}_k. \tag{2.28}$$

For each step $k = 1, 2, 3$, after solving (2.28) for $h^{n+\delta_k}$, we obtain $U^{n+\delta_k}$ and $V^{n+\delta_k}$ from (2.22) and (2.23), respectively.

For later comparison with the siRK3 scheme, we have also developed a semi-implicit leapfrog (hereafter siLF) scheme for the 2D shallow-water Eqs. (2.11)–(2.13). Following the derivations of the siRK3 scheme presented above, we can derive the siLF scheme as

$$U^{n+1} + \gamma^+ gH \frac{\partial h^{n+1}}{\partial x} = R_u, \tag{2.29}$$

$$V^{n+1} + \gamma^+ gH \frac{\partial h^{n+1}}{\partial y} = R_v, \text{ and} \tag{2.30}$$

$$\left(\frac{\partial^2}{\partial x^2} + \frac{\partial^2}{\partial y^2}\right)h^{n+1} - \frac{h^{n+1}}{gH(\gamma^+)^2} = \mathfrak{R}, \tag{2.31}$$

where

$$\gamma^+ \equiv (1 + \varepsilon_g)\Delta t \text{ and } \gamma^- \equiv (1 - \varepsilon_g)\Delta t, \tag{2.32}$$

and we have omitted the expressions for R_u , R_v , and \mathfrak{R} for brevity. To suppress the separation of the solutions at even and odd time steps due to the leapfrog scheme, a time filter (Asselin 1972) is applied at each time step. In this filter, the time average of a prognostic variable Ψ at time level n is given by

$$\overline{\Psi}^n = \Psi^n + \frac{\nu}{2}(\Psi^{n+1} - 2\Psi^n + \overline{\Psi}^{n-1}), \tag{2.33}$$

where ν is the filter parameter and the overbar denotes a time-averaged quantity. For the numerical accuracy and stability properties of the Asselin-filtered leapfrog scheme, see Durran (1999, 60–65).

b. Space discretization of the equations

We have already discretized the shallow-water Eqs. (2.11)–(2.13) in time using the siRK3 and siLF schemes, but we have left the horizontal coordinates in a differential form. In this section, we briefly describe the main

features of the horizontal grid and discretization used for the siRK3 scheme. An identical approach, not detailed here, is also used for the siLF scheme (2.29)–(2.31).

We employ an unstaggered A grid (Arakawa and Lamb 1977) to discretize the β -plane geometry, with the uniform grid size $\Delta x = \Delta y = \Delta$. The horizontal domain is bounded in x and y . The semidiscrete system made up of (2.28), (2.22), and (2.23) is solved over the rectangular grid domain $[nx, ny]$ that is surrounded by a boundary zone of six extra grid points that constitute an energy-absorbing boundary-relaxation zone (e.g., Kar and Turco 1995). We have employed second-order centered-difference schemes to discretize the spatial-derivative terms that appear in $(N_u, N_v, R_u, R_v, R_h,$ and $\mathfrak{R}_h)_k$ given by (2.19), (2.20), (2.25), (2.26), (2.27), and (2.28), respectively.

The Laplacian operator in (2.28) is discretized as

$$(\nabla^2 \Psi)_{ij} = \frac{1}{\Delta^2} (\Psi_{i+1,j} + \Psi_{i-1,j} + \Psi_{i,j+1} + \Psi_{i,j-1} - 4\Psi_{ij}), \tag{2.34}$$

using a compact five-point stencil. This particular choice helps eliminate grid-scale gravity wave noise on the unstaggered A grid as shown in Kar (2000). The resulting space-discrete form of the elliptic Eq. (2.28) is solved iteratively by a generalized conjugate residual (GCR) algorithm (Skamarock et al. 1997). The spatial derivatives of $h^{n+\delta_k}$ in (2.22) and (2.23) are also finite differenced using second-order centered schemes. Finally, to control nonlinear computational instability associated with the horizontal advection, a scale-selective spatial filter (Purser 1987) has been applied at each time step to u , v , and h . This particular filter is defined in the x direction as

$$\begin{aligned} \tilde{\Psi}_i = \frac{1}{4096} [& 2668\Psi_i + 1080(\Psi_{i+1} + \Psi_{i-1}) \\ & - 405(\Psi_{i+2} + \Psi_{i-2}) - 20(\Psi_{i+3} + \Psi_{i-3}) \\ & + 90(\Psi_{i+4} + \Psi_{i-4}) - 36(\Psi_{i+5} + \Psi_{i-5}) \\ & + 5(\Psi_{i+6} + \Psi_{i-6})], \end{aligned} \tag{2.35}$$

and defined similarly in the y direction. The spectral response of this filter displayed by the curve labeled (4, 1) in Fig. 1f of Purser (1987) shows the effective suppression of wavelengths between two and four grid intervals. No other numerical damping or diffusion has been used in the model.

c. Numerical results

We have implemented three time-difference schemes, namely, the expRK3, siRK3, and siLF

schemes in the shallow-water model described above. For numerical time integration, a forced initial-boundary value problem is set up on a limited-area, midlatitude β plane, with a time-dependent but stationary point source and point sink of mass of equal strength aligned symmetrically in the middle of the domain with $nx = ny = 100$ and $\Delta = 100$ km. The point source and sink of mass vary sinusoidally in time with a period of 2 days and are of maximum strengths ± 100 m min^{-1} . The β plane is centered at 45°N , with $f_0 = 1.03 \times 10^{-4} \text{ s}^{-1}$ and $\beta = 1.62 \times 10^{-11} \text{ m}^{-1} \text{ s}^{-1}$. The other parameters are $g = 9.81 \text{ m s}^{-1}$ and $H = 10$ km. Thus, the pure gravity wave speed is $c_g = 313.2 \text{ m s}^{-1}$, and the radius of deformation, $\lambda_R \equiv (gH)^{1/2}/f_0 = 3040$ km. The source and sink of mass are placed roughly one radius of deformation apart, at the grid points (34, 50) and (66, 50), respectively. The time integrations are started from rest and continued for 6 days.

For later convenience, we introduce a gravity wave Courant number (μ_g) and an advective Courant number (μ_a) defined as

$$\mu_g \equiv \frac{c_g \Delta t}{\Delta} \quad \text{and} \quad \mu_a \equiv \frac{V \Delta t}{\Delta}, \quad (2.36)$$

where V denotes the absolute magnitude of the maximum horizontal wind speed attained during the time integrations of the model. Also, let $(\Delta t)_{\text{expRK3}}$, $(\Delta t)_{\text{siRK3}}$, and $(\Delta t)_{\text{siLF}}$ denote the time steps used by the expRK3, siRK3, and siLF schemes, respectively.

For the expRK3 scheme, we set $(\Delta t)_{\text{expRK3}} = 6$ min. Then, using (2.36) one obtains $(\mu_g)_{\text{expRK3}} = 1.12 < 1.73$, which is required for linear computational stability (Durrant 1999, 68–69) of the free-surface gravity waves. For the siRK3 and siLF schemes, however, the choice of time steps is limited by the linear computational stability of horizontal advection, as both schemes are unconditionally stable, by design, for the free-surface gravity waves. We have tested a number of different values for $(\Delta t)_{\text{siRK3}}$ and $(\Delta t)_{\text{siLF}}$, but here we only show the results for $(\Delta t)_{\text{siRK3}} = (\Delta t)_{\text{siLF}} = 90$ min = $15(\Delta t)_{\text{expRK3}}$ and $(\Delta t)_{\text{siRK3}} = 180$ min = $30(\Delta t)_{\text{expRK3}}$. For such choices of time step, the corresponding gravity wave Courant numbers are obtained from (2.36) as $(\mu_g)_{\text{siRK3}} = (\mu_g)_{\text{siLF}} = 16.9 \gg 1$ and $(\mu_g)_{\text{siRK3}} = 33.8 \gg 1$. Thus, both the siRK3 and siLF schemes are unconditionally stable for the surface gravity waves. Here, the expRK3 scheme requires 1440 time steps to complete the 6-day time integration. With time steps of 90 and 180 min, the semi-implicit schemes require 96 and 48 time steps, respectively, to complete the 6-day time integration.

As indicated above, both the siRK3 and siLF schemes are conditionally stable for the horizontal ad-

vection in the model. Thus, the CFL restrictions for the siRK3 and siLF schemes are given by $(\mu_a)_{\text{siRK3}} < 1.73$ and $(\mu_a)_{\text{siLF}} < 1$, respectively. For the 6-day time integrations that we have carried out, the model-predicted, maximum current speed is $V \approx 13 \text{ m s}^{-1}$. Thus, from (2.36), the advective Courant numbers for the siRK3 scheme are given by $(\mu_a) \equiv 0.7$ and 1.4 for $(\Delta t)_{\text{siRK3}} = 90$ and 180 min, respectively. Similarly, the advective Courant number for the siLF scheme is given by $(\mu_a)_{\text{siLF}} \equiv 0.7$ for $(\Delta t)_{\text{siLF}} = 90$ min. Clearly, for the present horizontal resolution, the “largest” time steps for the siRK3 and siLF schemes are $(\Delta t)_{\text{siRK3}} = 180$ min and $(\Delta t)_{\text{siLF}} = 90$ min. Note that the uncentering parameter ε_g is set to zero for both the siRK3 and siLF schemes.

Figures 1, 2, and 3 show the expRK3, siRK3, and siLF scheme based shallow-water models predicted perturbation free-surface heights at day 1, day 2, and day 5 of the time integrations. Each figure consists of four panels: (a) for the expRK3 scheme with $(\Delta t)_{\text{expRK3}} = 6$ min; (b) and (c) for the siRK3 scheme with $(\Delta t)_{\text{siRK3}} = 90$ min and 180 min, respectively; and (d) for the siLF scheme with $(\Delta t)_{\text{siLF}} = 90$ min. The perturbation height field shows the time evolution (not the entire sequence) of a forced large-scale wave-one pattern that is influenced by the β effect. We notice that on day 1, the overall solution for the siRK3 scheme is reasonably close to that for the expRK3 scheme and the siLF scheme. On day 2, compared to day 1, we notice that the low and high centers have switched positions because of the 2-day periodicity of the mass-source and mass-sink terms. We also notice that except for some differences near the source and sink areas, the siRK3 solutions are again reasonably close to the expRK3 and siLF solutions. The same observation continues to hold acceptably well into day 5, as shown in Fig. 3. These results demonstrate that over a period of several days, the siRK3 scheme is numerically stable with a solution that is nearly as accurate as that of the expRK3 scheme, with the semi-implicit scheme using a time step that is an order of magnitude larger than that used by the fully explicit scheme. Note that the siLF scheme also performs acceptably well compared to both the expRK3 and siRK3 schemes.

Using the model-predicted u , v , and h , we have also computed a number of diagnostic quantities, namely, the area-integrated mass (M), total energy (E), and absolute potential enstrophy (Π) defined by

$$M \equiv \langle \xi \rangle, \quad E \equiv \left\langle \frac{1}{2} \xi (u^2 + v^2) + \frac{1}{2} g \xi^2 \right\rangle, \quad \text{and} \\ \Pi \equiv \left\langle \frac{1}{2\xi} \left(f + \frac{\partial v}{\partial x} - \frac{\partial u}{\partial y} \right)^2 \right\rangle, \quad (2.37)$$

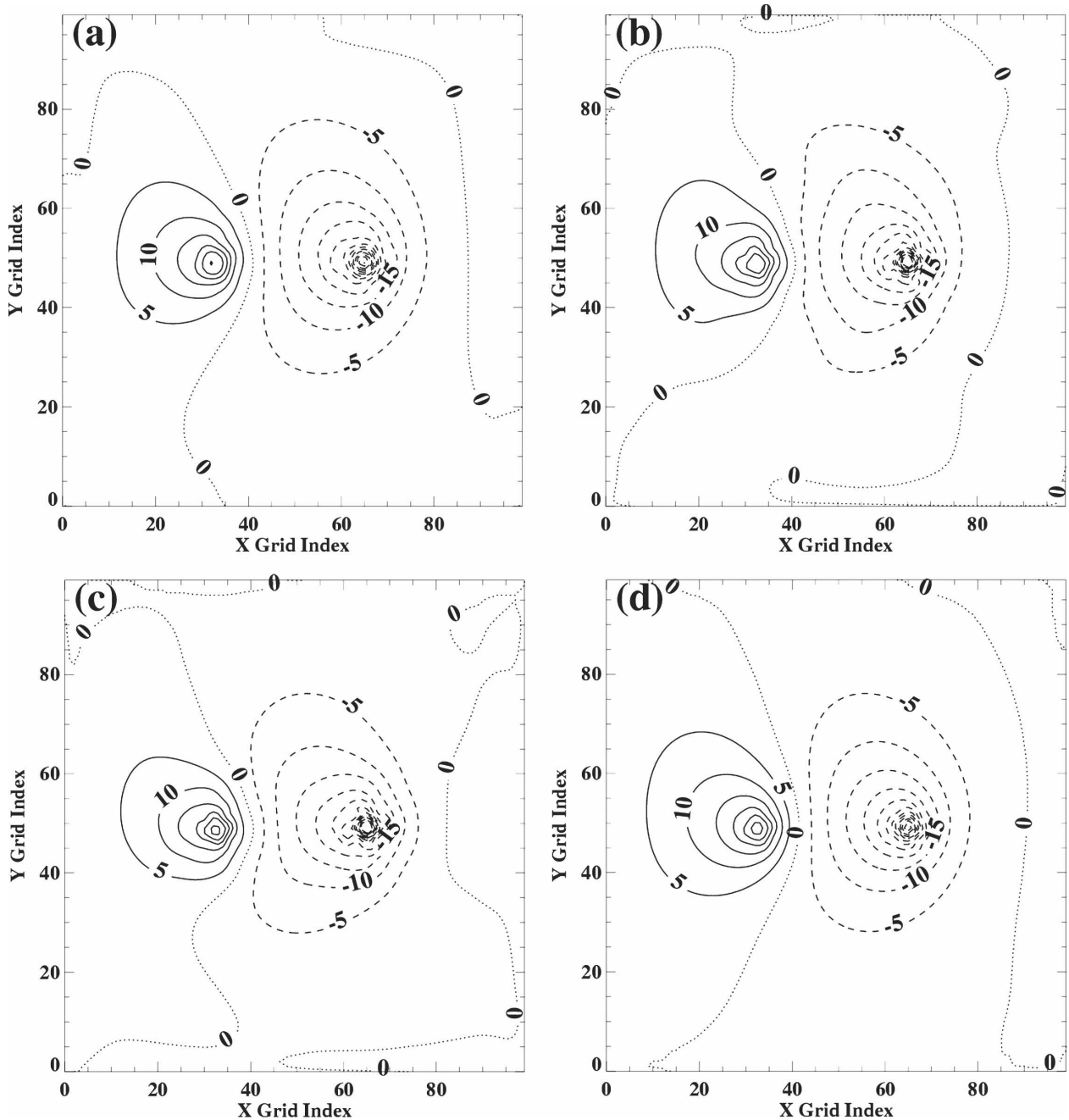


FIG. 1. Solution at day 1 of the 2D shallow-water model (a) using the explicit RK3 scheme with a time step of 6 min, (b) using the semi-implicit RK3 scheme with a time step of 90 min, (c) using the semi-implicit RK3 scheme with a time step of 180 min, and (d) using the semi-implicit leapfrog scheme with a time step of 90 min. Contours of perturbation height (m) are plotted at an interval of 5 m.

where

$$\langle \Psi \rangle \equiv \iint \Psi \, dx \, dy. \quad (2.38)$$

Note that by design of the spatial differencing, the area-integrated total mass is conserved in the time-continuous case. For the shallow-water equations in a

continuous form (2.11)–(2.13), it is readily verified that M , E , and Π are conserved in time, provided there are no friction and mass source and sink terms. Even though the current test involves a time-dependent source and sink of mass, it is of interest to look into the time series of M , E , and Π computed from the model solutions.

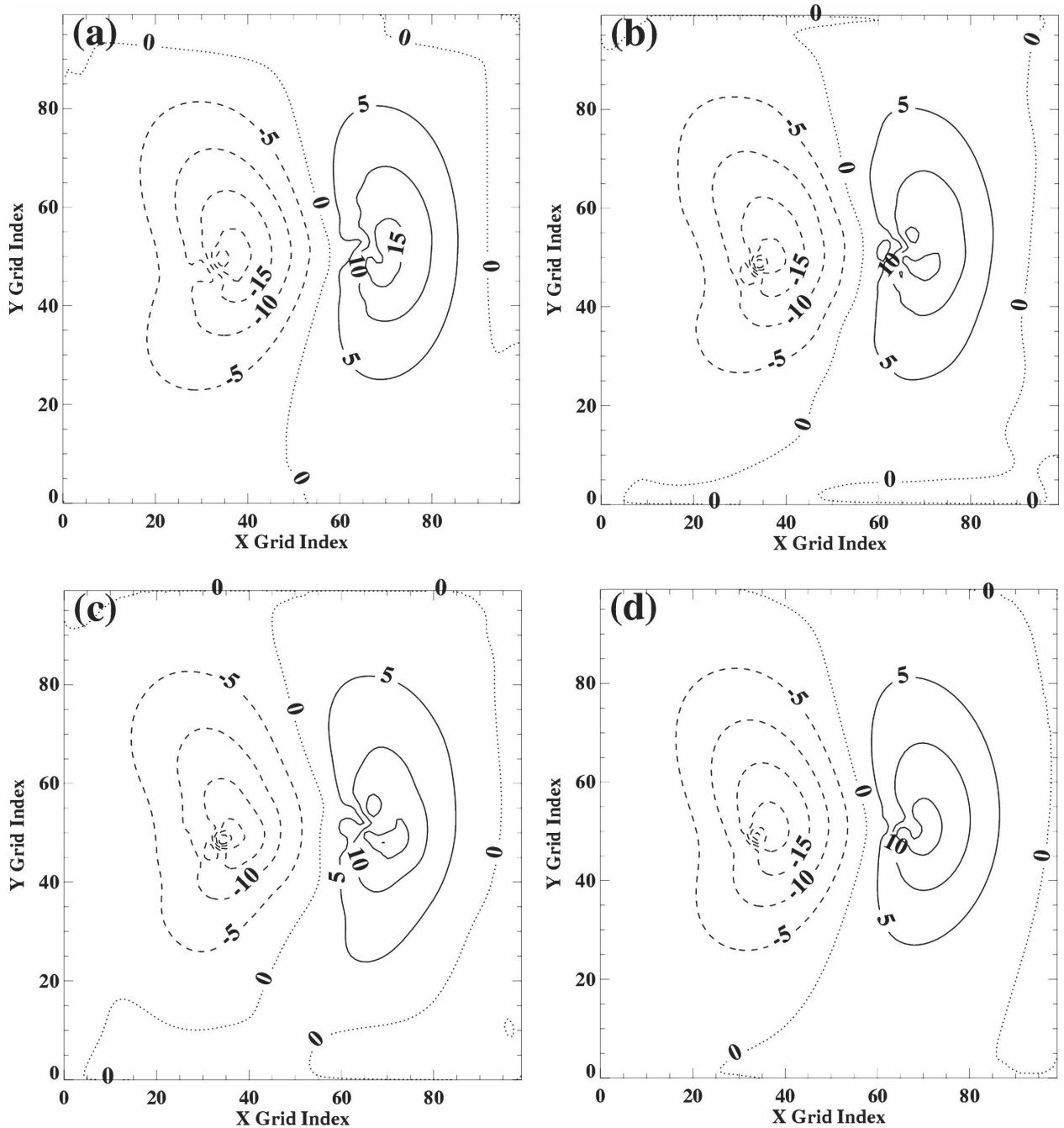


FIG. 2. As in Fig. 1 but valid at day 2 of the time integration.

Figure 4 shows the time series of the model-computed M , E , and Π for the `expRK3`, `siRK3`, and `siLF` schemes. The plotted variables are normalized by their respective initial values. The time variations of both M and E , irrespective of the schemes, are bounded and relatively small with a quasi-periodicity of 2 days. The `siRK3` and `siLF` solutions closely follow the `expRK3` solution, particularly in terms of phase. In

terms of amplitude, the `siRK3` and `siLF` schemes register slightly lower absolute magnitudes compared to the `expRK3` scheme. This particular aspect of the `siRK3` solution is slightly enhanced when the time step is increased. Figure 4c shows that the model-computed absolute potential enstrophy Π also remains bounded and shows very similar phase variations in time for all schemes. Compared with the `expRK3` and `siLF` schemes,

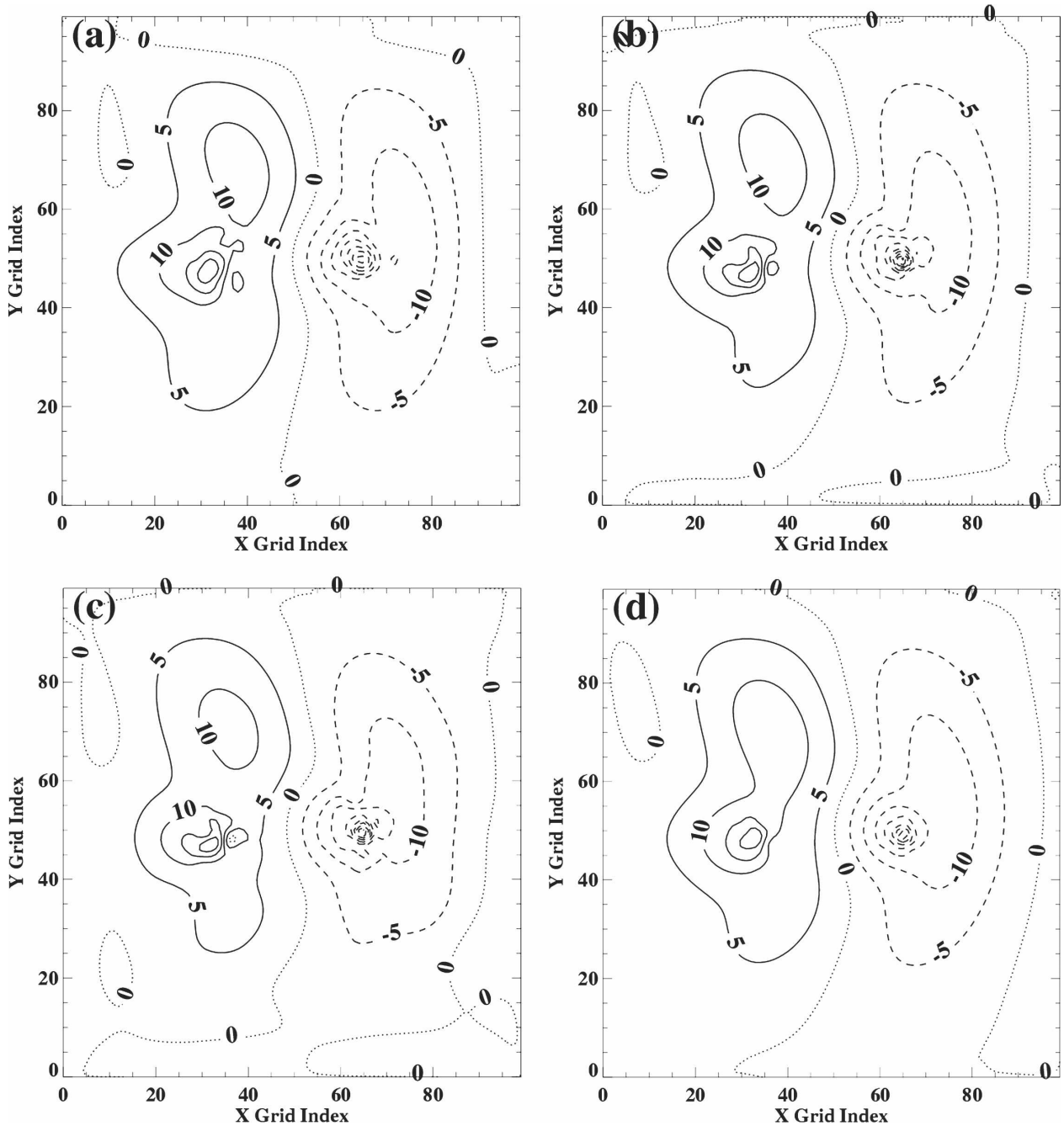


FIG. 3. As in Fig. 1 but valid at day 5 of the time integration.

the siRK3 scheme seems to incur a systematic increase in Π . Such an increase, however, amounts to about only 0.15% in the time-averaged sense.

Clearly, the sirk3 scheme allows for the use of relatively large time steps compared to the exprk3 scheme, but it has the computational burden of solving three elliptic equations per time step. To address the issue of computational efficiency, we have computed

the total CPU time used by the siRK3 scheme for the 6-day run and compared it with the same used by the exprk3 and siLF schemes. As indicated earlier, the elliptic equations associated with the siRK3 and siLF schemes are solved iteratively using a GCR algorithm (see Skamarock et al. 1997, p. 591), where the iterative-convergence parameter ϵ is set to a value 10^{-6} . The shallow-water model was run on a Dell desktop com-

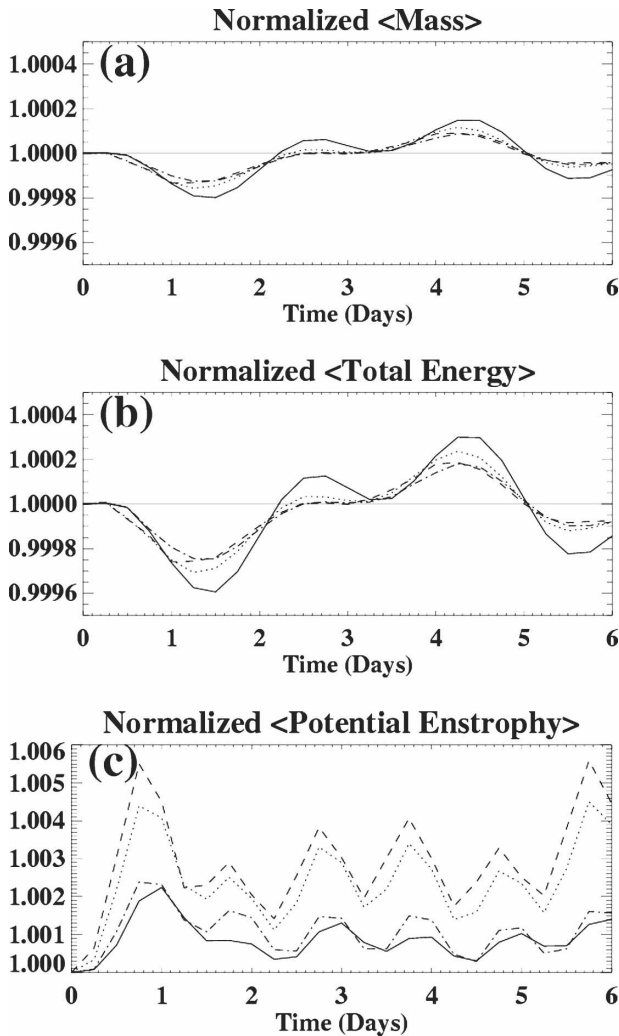


FIG. 4. Time evolution of the area-integrated (a) mass, (b) total energy, and (c) absolute potential enstrophy. Each quantity is normalized by its initial value. The solid curve is for the explicit RK3 scheme with $\Delta t = 6$ min. The dotted and dashed curves are for the semi-implicit RK3 scheme with $\Delta t = 90$ and 180 min, respectively. The dotted-dashed curve is for the semi-implicit leapfrog scheme with $\Delta t = 90$ min.

puter (Intel Pentium 4, 2.80 GHz) using Red Hat Linux version 3 as the operating system. The total CPU time used by the *expRK3* scheme, for a 6-day run of the shallow-water model is 28.42 s. The corresponding CPU times used by the *siRK3* scheme are 13.94 and 10.29 s for $(\Delta t)_{\text{siRK3}} = 90$ and 180 min, respectively. The total CPU time used by the *siLF* scheme is 7.87 s for $(\Delta t)_{\text{siLF}} = 90$ min. Thus, the *siRK3* scheme with a time step of 180 min costs nearly 30% more compared to the *siLF* scheme with a time step of 90 min. Note that the GCR solver used here does not include a preconditioner that could accelerate its convergence and

thereby potentially improve upon the current efficiency of the *siRK3* scheme compared to the *siLF* scheme.

3. Summary

In the framework of a two-dimensional shallow-water model in flux convergence form, a semi-implicit Runge–Kutta time-difference scheme has been developed. The proposed scheme essentially extends an established explicit third-order Runge–Kutta (*expRK3*) time-difference scheme into a semi-implicit Runge–Kutta (*siRK3*) scheme that employs (a) a second-order trapezoidal scheme for the gravity wave terms, at each of the three iterative steps of the third-order Runge–Kutta scheme, but (b) continues to employ the explicit third-order Runge–Kutta scheme for the nonlinear terms including horizontal fluxes of mass and momentum. A linear stability analysis of the proposed scheme is presented in the appendix. The *siRK3* scheme requires a two-dimensional Helmholtz-type elliptic equation to be solved at each iterative step of the scheme. A conjugate-residual solver without a preconditioner has been used in the model to solve the aforementioned elliptic equation.

The effectiveness of the *siRK3* scheme, compared to the *expRK3* and the semi-implicit (time filtered) leapfrog (hereafter *siLF*) schemes in terms of numerical stability, accuracy, and efficiency, is established through an idealized numerical time integration of the shallow-water model. The numerical results show that even though the *siRK3* scheme treats the gravity waves with second-order accuracy in time, compared to the third-order accuracy of the *expRK3* scheme, the *siRK3* provides a stable, reasonably accurate, and numerically efficient solution with relatively large time steps. However, the *siRK3* scheme costs about 30% more in terms of CPU time compared to the *siLF* scheme. The additional computational burden is perhaps bearable in view of the third-order accuracy in time obtained for horizontal advection using the *siRK3* scheme, compared to less than second-order accuracy in time for the same process using the Asselin-filtered *siLF* scheme.

The proposed *siRK3* scheme was implemented in the shallow-water equations in a flux convergence form. This ensures conservation of total mass; however, the same scheme can also be easily applied to the advective form of the shallow-water equations.

The proposed *siRK3* scheme can be implemented in three-dimensional hydrostatic and nonhydrostatic models, once the semi-implicit linearization of the appropriate governing equations is established. The proposed scheme can also be adapted to semi-Lagrangian dynamics, if we employ a backward-trajectory-based semi-

Lagrangian advection scheme to each of the three iterative steps of the scheme. Some of these issues will be addressed in the future.

Acknowledgments. The author is thankful to Drs. R. James Purser and Joseph Sela for helpful comments on the original draft, and Mary L. Hart for editorial improvements. The author greatly appreciates the reviewers' comments in significantly improving the paper.

APPENDIX

Linear Stability Analysis of the siRK3 Scheme

To perform a von Neumann stability analysis of the siRK3 scheme, let us substitute

$$L(\Psi) = i\alpha\Psi \quad \text{and} \quad N(\Psi) = i\beta\Psi \quad (\text{A.1})$$

into (2.10). Here, α and β denote the relatively high and low frequencies of Ψ , and $i \equiv \sqrt{-1}$. Then, (2.10) can be expanded into the following component steps:

$$(1 - i\delta_1\varepsilon_g^+\alpha\Delta t)\Psi^* = [1 + i\delta_1(\varepsilon_g^-\alpha\Delta t + \beta\Delta t)]\Psi^n, \quad (\text{A.2})$$

$$(1 - i\delta_2\varepsilon_g^+\alpha\Delta t)\Psi^{**} = (1 + i\delta_2\varepsilon_g^-\alpha\Delta t)\Psi^n + (i\delta_2\beta\Delta t)\Psi^*, \quad \text{and} \quad (\text{A.3})$$

$$(1 - i\varepsilon_g^+\alpha\Delta t)\Psi^{n+1} = (1 + i\varepsilon_g^-\alpha\Delta t)\Psi^n + (i\beta\Delta t)\Psi^{**}, \quad (\text{A.4})$$

where

$$\varepsilon_g^+ \equiv \frac{1}{2}(1 + \varepsilon_g) \quad \text{and} \quad \varepsilon_g^- \equiv \frac{1}{2}(1 - \varepsilon_g). \quad (\text{A.5})$$

Eliminating the variables Ψ^* and Ψ^{**} from (A.2)–(A.4), we can derive the (complex) amplification factor λ defined by

$$\lambda \equiv \Psi^{n+1}/\Psi^n, \quad (\text{A.6})$$

in terms of the constants ε_g^+ and ε_g^- , and the variables $\alpha\Delta t$ and $\beta\Delta t$. Note that for stability of the siRK3 scheme, one must satisfy the condition $|\lambda| \leq 1$.

When $\alpha \equiv 0$ and $\beta \neq 0$, (2.10) reduces to the expRK3 scheme with the amplification factor

$$\lambda = \left[1 - \frac{1}{2}(\beta\Delta t)^2 \right] + i \left[\beta\Delta t - \frac{1}{6}(\beta\Delta t)^3 \right]. \quad (\text{A.7})$$

This leads to

$$|\lambda|^2 = 1 - \frac{1}{12}(\beta\Delta t)^4 + \frac{1}{36}(\beta\Delta t)^6, \quad (\text{A.8})$$

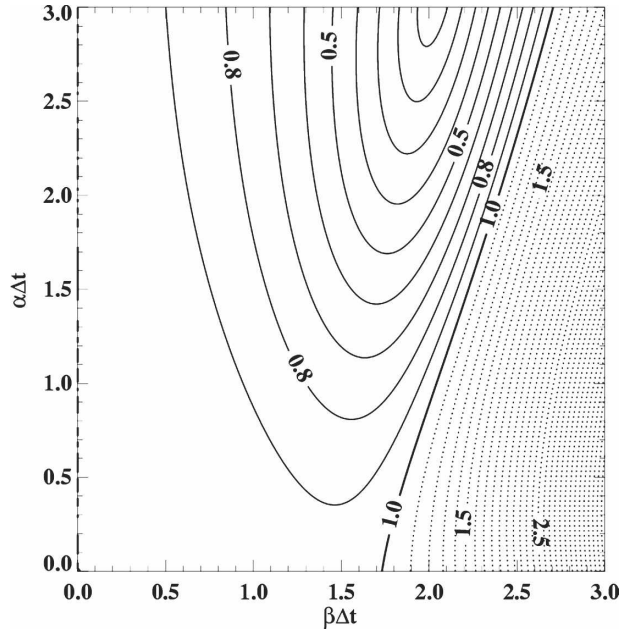


FIG. A1. The modulus of the amplification factor λ as a function of $\alpha\Delta t$ and $\beta\Delta t$ for the semi-implicit RK3 scheme applied to the oscillation equation: $d_t\Psi = i\omega\Psi$, where $\omega(= \alpha + \beta)$ is the angular frequency. The contour interval is 0.1. The solid and dashed contours, respectively, are used to display the stable ($|\lambda| \leq 1$) and unstable ($|\lambda| > 1$) regions of the $(\alpha\Delta t, \beta\Delta t)$ parameter space. When $\beta\Delta t = 0$, $|\lambda| = 1$ for all values of $\alpha\Delta t$, along the $\alpha\Delta t$ axis.

so that for the stability of the expRK3 scheme, $|\lambda| \leq 1$ or $|\beta\Delta t| \leq \sqrt{3} \approx 1.73$ must be satisfied.

However, when $\alpha \neq 0$ and $\beta \neq 0$, the algebraic expression (not shown) for $|\lambda|$ does not readily yield an explicit inequality in terms of $\alpha\Delta t$ and $\beta\Delta t$. To address this issue numerically, we have plotted the contours of $|\lambda|$ as a function of $\alpha\Delta t$ and $\beta\Delta t$ in Fig. A1. Here we have assumed $\varepsilon_g \equiv 0$, for simplicity. The dashed contours of $|\lambda|$ valued greater than unity display the unstable region. The region of stability is recognized by the solid contours of $|\lambda|$ valued less than unity. Clearly, the stable region is limited by $\beta\Delta t < 1.73$, for all values of $\alpha\Delta t$. Thus, the siRK3 scheme is conditionally stable with the stability restriction, $\beta\Delta t < 1.73$, which is essentially dictated by the explicit RK3 part of the scheme, as expected.

REFERENCES

Arakawa, A., and V. R. Lamb, 1977: Computational design of the basic dynamical processes of the UCLA general circulation model. *Methods in Computational Physics*, J. Chang, Ed., Vol. 17, Academic Press, 173–265.

Ascher, U. M., S. J. Ruuth, and R. J. Spiteri, 1997: Implicit–explicit Runge–Kutta methods for time-dependent partial differential equations. *Appl. Numer. Math.*, **25**, 151–167.

- Asselin, R., 1972: Frequency filter for time integrations. *Mon. Wea. Rev.*, **100**, 487–490.
- Butcher, J. C., 1964: Implicit Runge–Kutta processes. *Math. Comput.*, **18**, 50–64.
- , 1987: *The Numerical Analysis of Ordinary Differential Equations: Runge–Kutta and General Linear Methods*. John Wiley and Sons, 512 pp.
- Durran, D. R., 1999: *Numerical Methods for Wave Equations in Geophysical Fluid Dynamics*. Springer-Verlag, 465 pp.
- Gear, C. W., 1971: *Numerical Initial Value Problems in Ordinary Differential Equations*. Prentice-Hall, 253 pp.
- Kar, S. K., 2000: Stable centered-difference schemes, based on an unstaggered A grid, that eliminate two-grid interval noise. *Mon. Wea. Rev.*, **128**, 3643–3653.
- , and R. P. Turco, 1995: Formulation of a lateral sponge layer for limited-area shallow-water models and an extension for the vertically stratified case. *Mon. Wea. Rev.*, **123**, 1542–1559.
- Kwizak, M., and A. J. Robert, 1971: A semi-implicit scheme for grid point atmospheric models of the primitive equations. *Mon. Wea. Rev.*, **99**, 32–36.
- Purser, R. J., 1987: The filtering of meteorological fields. *J. Climate Appl. Meteor.*, **26**, 1764–1769.
- Robert, A. J., 1969: The integration of a spectral model of the atmosphere by the implicit method. *Proc. WMO–IUGG Symp. on Numerical Weather Prediction*, Vol. VII, Tokyo, Japan, Japan Meteorological Agency, 19–24.
- Skamarock, W. C., P. K. Smolarkiewicz, and J. B. Klemp, 1997: Preconditioned conjugate-residual solvers for Helmholtz equations in nonhydrostatic models. *Mon. Wea. Rev.*, **125**, 587–599.
- , J. B. Klemp, and J. Dudhia, 2001: Prototypes for the WRF (Weather Research and Forecasting) model. *Extended Abstracts, Ninth Conf. on Mesoscale Processes*, Fort Lauderdale, FL, Amer. Meteor. Soc., J1.5.
- Wicker, L. J., and W. C. Skamarock, 2002: Time-splitting methods for elastic models using forward time schemes. *Mon. Wea. Rev.*, **130**, 2088–2097.